Journal of the Optical Society of America B

OPTICAL PHYSICS

Carrier-envelope phase stability of a polarization-encoded chirped pulse Ti:Sapphire amplifier

R. S. Nagymihaly,[1,2,*] H. Cao,[1] P. Jojart,[1,2] M. Kalashnikov,[1,3] A. Borzsonyi,[1,2] V. Chvykov,[1] R. Flender,[2] M. Kovacs,[1,2] and K. Osvay[1]

[1]ELI-HU Non-Profit Ltd., Dugonics tér 13, 6720 Szeged, Hungary
[2]Department of Optics and Quantum Electronics, University of Szeged, P.O. Box 406, H-6701 Szeged, Hungary
[3]Max Born Institute for Nonlinear Optics and Short Pulse Spectroscopy, Max-Born-Strasse 2a, 12489 Berlin, Germany
*Corresponding author: roland.nagymihaly@eli-alps.hu

The scheme of polarization-encoded chirped pulse amplification (PE-CPA) reduces the gain narrowing effect in Ti:Sapphire (Ti:Sa) amplifiers by utilizing both crystal axes of Ti:Sa. Hence, the carrier-envelope phase (CEP) of a PE-CPA pulse originates from two othogonal polarization directions. The CEP stability of PE-CPA pulses was investigated for various amplification conditions by varying the pump pulse energy. The CEP stability is directly compared to the conventional CPA scheme under the same laser parameters. A quasi-common-path interferometer was realized inside a four-pass amplifier stage, ensuring exceptional geometrical path length stability and high spectral phase sensitivity. The spectral phase noise of PE-CPA pulses showed a minor increase of 4 mrad compared to the conventional scheme, while at unsaturated amplification of a net gain of 13, it revealed a CEP stability better than 63 mrad.   © 2018 Optical Society of America

1. INTRODUCTION

Ti:Sapphire (Ti:Sa) gain material is used in most ultrahigh peak power chirped pulse amplifier (CPA) laser systems because of its broad gain bandwidth and exceptional physical properties, including its high room temperature and extraordinary cryogenic thermal conductivity [1–5]. The carrier-envelope phase (CEP) stability of ultrafast amplifier systems is one of the main requisites for the study of extreme nonlinear optical phenomena. High intrinsic CEP stability of amplifier systems can only be obtained by careful design and realization of the amplification stages, which requires specialized knowledge regarding the CEP drift and noise. For example, the CEP stability of water and cryogenically cooled multipass Ti:Sa amplifier stages has been recently investigated by using spectrally resolved interferometry [6,7]. The limit of CEP stabilization in Ti:Sa-based mJ-class CPA systems has been found to be around 100 mrad RMS by using quite complex electronics [8]. However, gain-narrowing and gain-shifting effects still prevent the compressed pulses reaching the few-cycle regime, which is favorable for numerous scientific areas, e.g., attosecond science [9,10], and even laser-driven particle acceleration [11].

The novel scheme of polarization-encoded CPA (PE-CPA) was recently demonstrated and is capable of providing a gain bandwidth that supports few-cycle pulses after amplification and compression [12].

In a PE-CPA, contrary to a conventional CPA, both π- and σ-axes of the Ti:Sa crystals are used, leading to the reshaping of the gain spectrum. The polarization state of the seed spectrum is encoded before amplification using the optical rotatory dispersion (ORD) effect in a quartz crystal [13,14]. The central part of the seed spectrum is oriented close to the σ-axis, while the spectral wings are rotated towards the π-axis (Fig. 1). This results in the wings being more intensively amplified than the center of the spectrum and thus compensates for gain narrowing. The polarization vectors of the different spectral components are then decoded by using a quartz crystal with an opposite ORD sign. The spectral encoding and decoding can be tuned with half-wave plates, designed for a broad spectral range, before and after the amplifier to shape the output spectral profile. Birefringence in Ti:Sa causes group delay (GD) difference between the σ- and π-components, which is
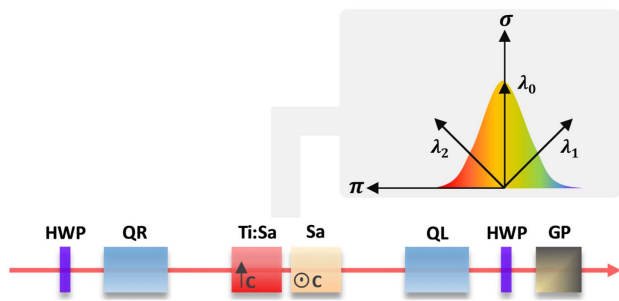
Fig. 1. Scheme of the polarization-encoded amplification process where HWPs are the broadband half-wave plates, QR and QL the right and left rotating quartz crystals, respectively, GP is the Glan polarizer, and C is the crystal axis orientation in case of the Ti:Sa–Sa pair. λ_0, λ_1, and λ_2 are related to the central, blue side, and red side wavelength values of the seed spectrum, respectively.

compensated by an undoped Sa crystal with the same thickness as the Ti:Sa gain medium, but with orthogonal orientation.

PE amplification utilizes gain cross sections for both π- and σ-axes in the Ti:Sa crystal and manipulation of the polarization directions of seed pulses, and thus, the amplification process could induce unforeseen effects on the decoded output phase stability. Phase stability is a necessary parameter for full control over the electric field of pulses and thus is highly important for investigating the stability of the spectral phase, including the CEP during PE amplification.

2. EXPERIMENTAL

The technique of spectrally resolved interferometry (SRI) has been chosen, as it is the only tool that is inherently capable of measuring directly the CEP stability of a single component independently of the rest of the system [15–17]. A Ti:Sa CPA front end served as the light source, with 2 mJ pulse energy and 40 ps temporal duration. The pulses were directed to an Öffner-type double-pass stretcher and further stretched to

200 ps. The pulses were injected into a Ti:Sa booster amplifier with a three-pass bow-tie geometry and amplified to 1 mJ energy with part of the pump pulses from a 0.5 J Quanta-Ray (Spectra-Physics) nanosecond laser. The beam diameter was resized after the booster amplifier for optimal mode matching in the PE amplifier stage.

A simple two-arm interferometer is normally sensitive enough to measure the amplification effects on the spectral phase. However, when the beam path length in an interferometer reaches several meters, significant geometrical path length fluctuations can arise during the measurement, leading to large levels of background phase noise, even with stable optomechanical components and a fully covered optical setup. For this reason, a quasi-common-path interferometer was realized, in which the sample beam propagates 5 mm above the reference beam and follows the same path. Both beams are reflected from the same mirrors inside the amplifier. The sample and reference pulses are generated through the reflections from the two surfaces of a beam splitter, where a sample-to-reference ratio of 1/10 was chosen. Both sample and reference pulses pass through the quartz crystals and half-wave plates, while only the sample passes through the Ti:Sa–Sa pair. After the amplifier, the path of the sample and reference pulses are separated only for a short distance to adjust the necessary timing for achieving spectral interference (Fig. 2).

The four-pass PE amplifier was designed for a small signal gain of around 10 to match the intensity of the amplified sample pulse with that of the reference pulse. The seed energy in the sample arm was around 10 μJ. The Ti:Sa crystal (thickness of 9 mm) was pumped from both sides, and the transmitted pump fractions were backreflected for a total pump absorption ratio of 97%. The polarization states were decoded by using a left rotating quartz crystal and a second half-wave plate in both arms. The half-wave plate was tuned to extract a linearly polarized pulse when the optimal energy and spectral bandwidth were obtained. The sample and reference pulses were then separated by a mirror, which only reflected the sample pulse.
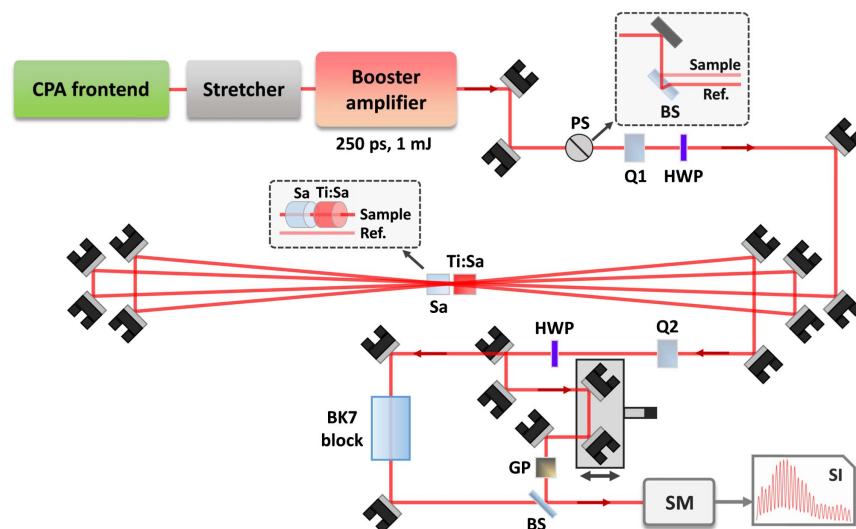

Fig. 2. Schematic picture of the experimental arrangement. PS is a periscope with beam splitting, Q1 and Q2 are right and left rotating quartz crystals, HWPs are broadband half-wave plates, GP is a Glan polarizer, SM is a spectrometer, and SI is a spectral interference.

The sample pulse was sent through a Glan polarizer to keep the p-polarized component while the reference pulse was sent through a BK7 glass block, compensating for the GD dispersion difference relative to the sample pulse due to the Ti:Sa–Sa pair and the Glan polarizer. Finally, the pulses were recombined by a beam splitter and sent to the entrance slit of an Ocean Optics HR4000 high-resolution spectrometer operating in triggered mode. Visibility of the spectral interference fringes was optimized by using reflective neutral density (ND) filters.

The interference fringes were monitored and recorded by an in-house code, which is capable of evaluating the fringes in real time so that during the measurement, the GD changes can reveal directly the stability of the interferometer. Complete evaluation of the fringes used the Fourier-transformation method [16,17], ensuring a high level of accuracy and freedom for optimization for individual fringe pattern analysis.

3. RESULTS

The application of a quasi-common-path optical arrangement results in the measurement of the effects inside the Ti:Sa–Sa pair and the dispersion compensation part of the interferometer. Kerr-type nonlinear phase accumulation is negligible in all optics in the setup due to the low energy in both arms and the large amount of chirp present in the stretched pulses. The temperature change in optical elements other than the Ti:Sa–Sa pair, which are water-cooled, is also negligible. Thus, the measured spectral phase changes can be solely attributed to the Ti:Sa–Sa pair and the residual path length fluctuation of the dispersion control stage. The latter is the major source of the error in the measured phase noise in all cases. Other than the inherent noise in the setup due to residual geometrical path length and beam direction fluctuations, the detection limit of the spectrometer and precision of the evaluation method defined the sensitivity of the experiment. The measured spectral phase fluctuation was first carefully analyzed, and it was found that the pulse-to-pulse change of the spectral phase had an undetectable slope throughout the pulse spectrum for all measurements. Based on these observations and the nature of the quasi-common-path measurement, all the presented phase-noise values in this paper can be interpreted as a pessimistic estimate on the increase of the CEP noise due to the amplification process. Similar conclusions have also been made where the degradation of the CEP stability was investigated by spectral interferometry in a hollow-core fiber nonlinear pulse compression stage [18].

The absolute sensitivity of the interferometer was determined by measuring the phase noise by letting the sample and reference pulses propagate through the nonpumped PE amplifier. Special care was taken to eliminate all environmental noise sources during the measurements, including air conditioning and mechanical vibrations. The background spectral phase noise RMS was found to be not greater than 38 mrad in the worst case. The phase stability of the PE amplifier was then compared to conventional amplification at the same pump energy level by converting the PE amplifier to a regular Ti:Sa amplifier with the same seed and pump conditions. Spectral phase fluctuations were measured for 10,000 pulses, and the shot-to-shot RMS noise was calculated for both cases
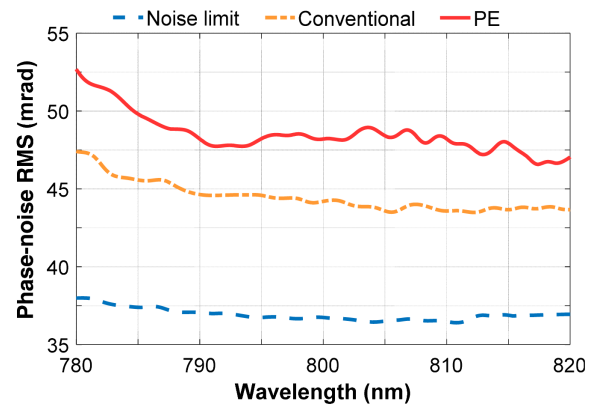

Fig. 3. Shot-to-shot spectral phase-noise RMS for different wavelengths: measurement noise (noise limit, blue), standard amplification (conventional, orange), and polarization-encoded amplification (PE, red) at the same pump energy level (64 mJ).

without averaging (Fig. 3). The spectral phase noise RMS was calculated for all frequencies covered by the spectral content of the measured pulses. A phase-noise difference of around 4 mrad was found between the conventional and PE amplification, proving that the two amplifier schemes have nearly the same phase stability. The slight difference can be attributed to the polarization encoding of the seed spectrum.

Dependence of the phase noise on the pump energy and thus on the gain was also investigated in the PE amplifier. The pump energy was tuned from 64 to 86 mJ, while the gain changed from 10 to 13 with the seed pulse energy kept at the same level. The phase fluctuations were measured for 10,000 pulses, and the shot-to-shot noise was calculated again, without averaging, and is shown in Fig. 4.

There was no noticeable change in the phase-noise RMS caused by increasing the pump energy from 64 to 71 mJ. However, at 79 and 86 mJ energies, a slight increase was found for all frequencies, which could imply that the CEP degradation is nonlinear to the gain increase. The maximum phase noise was measured close to the central wavelength with a value of about 63 mrad at 86 mJ pump energy. Stability of the pump
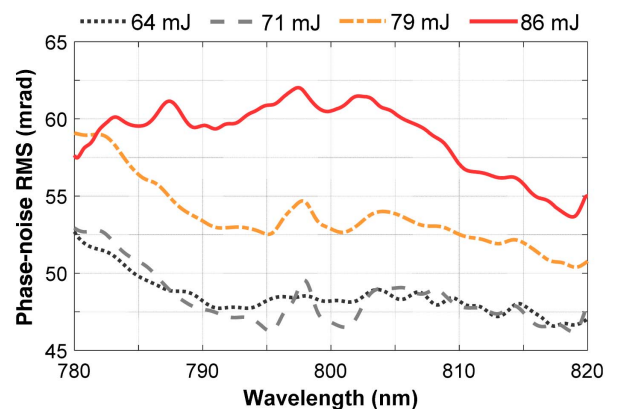

Fig. 4. Shot-to-shot spectral phase-noise RMS for different wavelengths, measured for the operation of the PE amplifier at different pump energies.
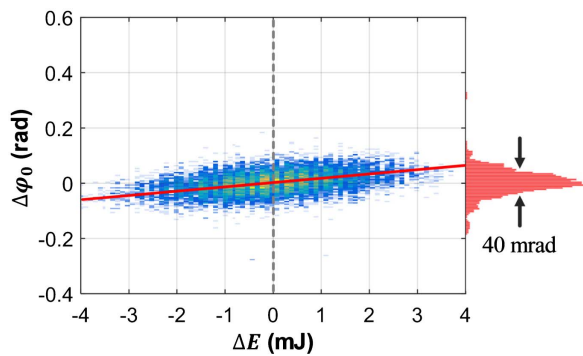
Fig. 5. Shot-to-shot phase change at the central wavelength in the function of the shot-to-shot pump energy fluctuation in case of 86 mJ pumping. A linear fit has a gradient of 23.5 mrad/mJ (red line). A histogram of the cross section at zero energy fluctuation is shown on the right side of the figure, with an RMS value of 40 mrad.

pulse energy was also monitored during the phase measurements. The energy fluctuation was compared to the phase variation, and good correlation was found between the data sets (Fig. 5). The pump energy fluctuations are coupled to phase noise via the gain and thermally induced refractive index changes. Utilization of both axes of Ti:Sa for amplification leads to different gain factors and refractive index changes for the two polarization states.

It is reasonable that the phase stability of the PE amplifier will degrade more when compared to conventional amplifiers, as the sensitivity of the refractive index to gain for σ-axis of Ti:Sa is 4 times that of the π-axis, as reported in [19]. Complete and precise characterization of this effect needs further investigation. A correlation was found for all measurements with PE amplification by comparing the pump energy fluctuations to the spectral phase changes. Linear fits to the $\Delta\varphi_0(\Delta E)$ distributions resulted in an averaged gradient of 20 mrad/mJ with a standard deviation of 4 mrad/mJ for measurements with different pump energies. This gradient shows the energy-phase coupling for four passes in the amplifier. The effect can be clearly seen in Fig. 4, where an increase in the pump energy, and thus the shot-to-shot fluctuation of its value, results in an elevation of the RMS phase noise across the whole spectrum.

4. SUMMARY AND DISCUSSION

The spectral phase fluctuations in a polarization-encoded chirped pulse Ti:Sa power amplifier stage have been measured with spectrally resolved interferometry. A quasi-common-path interferometer was realized with spatial separation of the reference and sample pulses, resulting in unprecedented sensitivity on the spectral phase changes. The spectral phase difference determined by extracting the phase content from the interference fringes was carefully analyzed, and no significant slope was found across the whole frequency spectrum. The quasi-common-path setup and the experimental findings enable ascribing all the phase changes exclusively to CEP variations.

Background measurements showed an absolute sensitivity noise level of around 38 mrad. Phase stability of the PE

amplifier has been compared to the conventional amplification with the same seed and pump parameters, and only a 4 mrad increase throughout the frequency spectrum was found in the case of the PE amplifier. The PE amplifier was also investigated for pumping with different pulse energies, where a slight increase in the phase noise was observed for higher pump energies and gain. The measured phase noise can be overestimated at the lower edge of the spectral range due to lower visibility of the fringes, and thus higher intrinsic noise of the evaluation. Pump energy fluctuations were compared to the phase variation, which showed a clear correlation and an increasing tendency with pump energy was found for the coupling between them. The CEP noise measured in this work is caused by the change of refractive indices along the two crystal axes with temperature and population inversion. These changes increase with stored pump energy density, and so their shot-to-shot fluctuation with the absolute pump energy jitter, similar to the conventional Ti:Sa amplifier schemes. However, upon PE amplification, the relative change of the two refractive indices at each crystal axis must be added. Hence, the CEP noise, in addition to the temperature-related contribution, will experience a negligible influence from the saturation effect. Since the stored pump energy is more effectively consumed in the saturation regime, the gain is more linear to the pump fluence, which results in a decreasing CEP noise related to the gain.

In conclusion, the PE process by the same laser parameters degrades the CEP stability only by a few milliradians when compared to conventional Ti:Sa amplification. Therefore, polarization-encoded amplification in Ti:Sa could be employed in CEP-stable high-energy CPA and double CPA systems as a substitute for conventional Ti:Sa amplifiers supporting significantly shorter pulses after compression, without additional notable effort for CEP stabilization. Based on these results, energy stability of the pump laser is a key point in keeping the operation of the amplifier phase stable. Thermally originated CEP drift and noise during the amplification is also sensitive to the pump energy stability. The increasing contribution of the pump energy fluctuation to the phase noise means it is highly advantageous to use diode-pumped solid-state lasers instead of traditional flashlamp-pumped models for driving the PE amplifier. Spectrally resolved investigation of the effect of population inversion on the refractive index is necessary to completely understand the phase changes during PE amplification, as the refractive index changes are different for the two axes of the Ti:Sa crystal.

REFERENCES

1. P. F. Moulton, "Spectroscopic and laser characteristics of Ti:Al₂O₃," J. Opt. Soc. Am. B **3**, 125–133 (1986).
2. D. C. Brown, "The promise of cryogenic solid-state lasers," IEEE J. Sel. Top. Quantum Electron. **11**, 587–599 (2005).

3. M. Kalashnikov, K. Osvay, and W. Sandner, "High-power Ti:Sapphire lasers: temporal contrast and spectral narrowing," Laser Part. Beams **25**, 219–223 (2007).

4. Y. Chu, X. Liang, L. Yu, Y. Xu, L. Xu, L. Ma, X. Lu, Y. Liu, Y. Leng, R. Li, and Z. Xu, "High-contrast 2.0 Petawatt Ti:sapphire laser system," Opt. Express **21**, 29231–29239 (2013).

5. Z. Gan, L. Yu, S. Li, C. Wang, X. Liang, Y. Liu, W. Li, Z. Guo, Z. Fan, X. Yuan, L. Xu, Z. Liu, Y. Xu, J. Lu, H. Lu, D. Yin, Y. Leng, R. Li, and Z. Xu, "200 J high efficiency Ti:sapphire chirped pulse amplifier pumped by temporal dual-pulse," Opt. Express **25**, 5169–5178 (2017).

6. A. Börzsönyi, R. S. Nagymihaly, and K. Osvay, "Drift and noise of the carrier-envelope phase in a Ti:sapphire amplifier," Laser Phys. Lett. **13**, 015301 (2016).

7. R. S. Nagymihaly, P. Jojart, A. Borzsonyi, and K. Osvay, "Spectral phase noise analysis of a cryogenically cooled Ti:Sapphire amplifier," Opt. Express **25**, 6690–6699 (2017).

8. F. Lücking, V. Crozatier, N. Forget, A. Assion, and F. Krausz, "Approaching the limits of carrier-envelope phase stability in a millijoule-class amplifier," Opt. Lett. **39**, 3884–3887 (2014).

9. F. Krausz and M. Ivanov, "Attosecond physics," Rev. Mod. Phys. **81**, 163–234 (2009).

10. S. Kühn, M. Dumergue, S. Kahaly, S. Mondal, M. Füle, T. Csizmadia, B. Farkas, B. Major, Z. Várallyay, F. Calegari, M. Devetta, F. Frassetto, E. Månsson, L. Poletto, S. Stagira, C. Vozzi, M. Nisoli, P. Rudawski, S. Maclot, F. Campi, H. Wikmark, C. L. Arnold, C. M. Heyl, P. Johnsson, A. L'Huillier, R. Lopez-Martens, S. Haessler, M. Bocoum, F. Boehle, A. Vernier, G. Iaquaniello, E. Skantzakis, N. Papadakis, C. Kalpouzos, P. Tzallas, F. Lépine, D. Charalambidis, K. Varju, K. Osvay, and G. Sansone, "The ELI-ALPS facility: the next generation of attosecond sources," J. Phys. B **50**, 132002 (2017).

11. E. N. Nerush and I. Yu. Kostyukov, "Carrier-envelope phase effects in plasma-based electron acceleration with few-cycle laser pulses," Phys. Rev. Lett. **103**, 035001 (2009).

12. M. Kalashnikov, H. Cao, K. Osvay, and V. Chvykov, "Polarization-encoded chirped pulse amplification in Ti:sapphire: a way toward few-cycle petawatt lasers," Opt. Lett. **41**, 25–28 (2016).

13. C. Ye, "Wavelength-tunable spectral filters based on the optical rotatory dispersion effect," Appl. Opt. **45**, 1162–1168 (2006).

14. S. Zheng, W. Chen, Y. Cai, X. Lu, G. Zheng, J. Li, and S. Xu, "Intra-cavity spectral shaping based on optical rotatory dispersion in a broadband Ti:S regenerative amplifier," Laser Phys. Lett. **12**, 085301 (2015).

15. A. Borzsonyi, A. P. Kovacs, and K. Osvay, "What we can learn about ultrashort pulses by linear optical methods," Appl. Sci. **3**, 515–544 (2013).

16. L. Lepetit, G. Cheriaux, and M. Joffre, "Linear techniques of phase measurement by femtosecond spectral interferometry for applications in spectroscopy," J. Opt. Soc. Am. B **12**, 2467–2474 (1995).

17. C. Dorrer and F. Salin, "Spectral resolution and sampling issues in Fourier-transform spectral interferometry," J. Opt. Soc. Am. B **15**, 2331–2337 (1998).

18. F. Lücking, A. Trabattoni, S. Anumula, G. Sansone, F. Calegari, M. Nisoli, T. Oksenhendler, and G. Tempea, "In situ measurement of nonlinear carrier-envelope phase changes in hollow fiber compression," Opt. Lett. **39**, 2302–2305 (2014).

19. K. F. Wall, R. L. Aggarwal, M. D. Sciacca, H. J. Zeiger, R. E. Fahey, and A. J. Strauss, "Optically induced nonresonant changes in the refractive index of $Ti:Al_2O_3$," Opt. Lett. **14**, 180–182 (1989).